Research Article Vol. 57, No. 1 / January 1 2018 / Applied Optics 25

applied optics

Numerical simulation and design of an apodized diffractive optical element composed of open-ring zones and pinholes

Tao Liu, Lingjie Wang, Jizhen Zhang, Qiang Fu, and Xin Zhang*

Key Laboratory of Optical System Advanced Manufacturing Technology, Changchun Institute of Optics and Fine Mechanics and Physics, Chinese Academy of Sciences, Changchun 130033, China
**Corresponding author: optlab@ciomp.ac.cn*

Received 28 April 2017; revised 13 September 2017; accepted 11 October 2017; posted 28 November 2017 (Doc. ID 294893); published 19 December 2017

In this paper, we investigate the relationship between open-ring zones of the Fresnel zone plate and the pinhole rings of photon sieves (PSs). Numerical simulations show that the normalized diffraction fields near the focal point of an individual pinhole ring and the circular open-ring zone are the same. It is confirmed that the maximum diffraction efficiency of an open-ring zone is higher than that of the traditional pinhole ring. Meanwhile, pinhole rings have more flexibility for apodization filtering. Based on these key findings, we propose the design theory of an apodized diffractive optical element comprised of open-ring zones and pinholes. To validate the theory, we developed a design example. Compared with traditional apodized PSs, the new apodized diffractive element has a 50.19% higher energy efficiency, and the minimum pinhole size is enlarged by 30.77%.

OCIS codes: (050.0050) Diffraction and gratings; (050.1940) Diffraction; (050.1965) Diffractive lenses; (110.0110) Imaging systems; (330.7321) Vision coupled optical systems.

https://doi.org/10.1364/AO.57.000025

1. INTRODUCTION

Fresnel zone plates (FZPs) and photon sieves (PSs) are two key imaging elements in high-resolution x-ray microscopy, extreme ultraviolet (EUV) lithography, and ultralarge membrane PS telescopes [1–7]. Compared with traditional FZP, PS increased the structure size by a d/w factor of 1.53, 3.51, and 5.51 [8–10]. The size of the pinholes and the underlying FZP zone are d and w, respectively. Both FZP and PS have circular diffraction structures with radially decreasing size. There have been many studies to increase the imaging resolution, suppress the sidelobe, and reduce the manufacturing difficulty of these diffractive optical elements (DOEs). Some researchers proposed a compound FZP that combines the first and higher-order diffraction open-ring zones [11,12]. Similarly, compound PSs, which combine PS and high-order FZP open-ring zones for the inner and outer zones, were designed for hard-x-ray nanofocusing [13].

In this paper, we discuss and compare analytical descriptions of the diffracted fields of the FZP's open-ring zones and the PS's pinhole rings. Figure 1 shows the schematic views of one open-ring zone of FZP and one pinhole ring of PS.

To the best of our knowledge, our work is the first to discuss the nature of the relationship between open-ring zones of FZP and the pinhole rings of PS. By treating all of the pinholes in a ring zone as a single unity, we proved that the normalized diffraction field near the focal point of a pinhole ring is the same as that of the circular open ring zone. Investigations also show that the maximum diffraction efficiency of an open-ring zone is 50.19% higher than that of the traditional $d/w = 1.53$ pinhole ring. Meanwhile, combined with the pinhole density modulation and pinhole size, PS has more flexibility for the apodization filtering. Based on these key findings, we proposed the design theory of apodized DOEs composed of open-ring zones and pinholes. In order to validate the theory, we design a high-performance apodized DOE that combines an inner open-ring zone and outer pinhole ring zone. In our design example, we first determine the apodized pupil function and element diameter. Investigations show that the compound apodized DOE designed with our proposed method has the maximum diffraction efficiency. Meanwhile, the structure sizes for the outer pinhole ring zone have been enlarged by a $d/w = 2.0$ factor in order to relax the fabrication requirements. More importantly, the normalized diffracted field near the focal point of this apodized DOE is the same as the apodized PS (APS), which means that the properties of high-spatial resolution and sidelobe suppression are maintained.

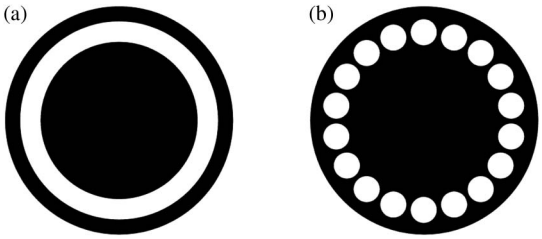

Fig. 1. Schematic view of (a) one open-ring zone of FZP and (b) one pinhole ring of PS.

2. DIFFRACTED FIELD OF OPEN-RING ZONE AND INDIVIDUAL PINHOLE RING

First, we investigate the diffracted field near the focal point of the nth open-ring zone of an FZP. It is perpendicularly illuminated by a plane wave. As shown in Fig. 2, f is the focal length of the FZP, and r_n is the radius at the center of the underlying nth zone.

From the Rayleigh–Sommerfeld diffraction integral, it has been deduced in [14] that the rotationally symmetric diffracted field $U_n(R)$ for the on-axis field is

$$U_n(R) = \frac{2f}{f_n}\exp\left[jk\left(f_n + \frac{R^2}{2f_n}\right)\right]J_0\left(\frac{kr_n}{f_n}R\right)\sin\left(\frac{k}{2}\frac{d_n}{f_n}\right), \quad (1)$$

where $f_n = (f^2 + r_n^2)^{1/2}$, $k = 2\pi/\lambda$ is the wavenumber. It should be noted that d_n is the half-width of the nth open-ring zone in the s coordinate, where $s = r^2$. That is, $d_n = \frac{1}{2}(b_n^2 - a_n^2)$, where a_n and b_n are the radii of the lower and upper edges of the nth open-ring zone in the r coordinate. These two radii can also be expressed as $a_n = r_n - \frac{d_{nF}}{2}$ and $b_n = r_n + \frac{d_{nF}}{2}$, where d_{nF} is the width of the nth open-ring zone in the r coordinate. By taking these relations into Eq. (1), and substituting the subscript n in the above expressions by m, we obtain

$$U_m(R) = 2\sin\left(\frac{k}{2}\frac{d_{mF}r_m}{f_m}\right)\frac{f}{f_m}\exp\left[jk\left(f_m + \frac{R^2}{2f_m}\right)\right]J_0\left(\frac{kRr_m}{f_m}\right). \quad (2)$$

Considering that the width of the mth local Fresnel ring zone $w_m = \lambda f_m/(2r_m)$, Eq. (2) can be changed to

$$U_{mF}(R) = E_{mF}\frac{f}{f_m}\exp\left[jk\left(f_m + \frac{R^2}{2f_m}\right)\right]J_0\left(\frac{kRr_m}{f_m}\right), \quad (3)$$

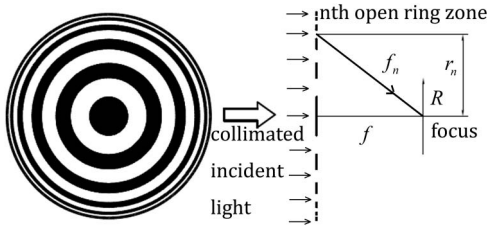

Fig. 2. Schematic view of an FZP and the focusing of the nth open-ring zone of the FZP.

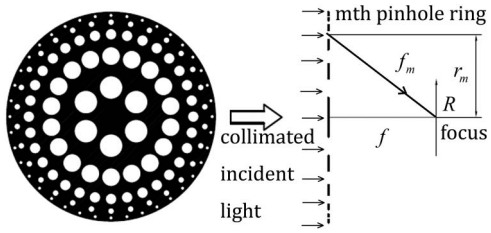

Fig. 3. Schematic view of a PS and the focusing of the pinholes in the mth ring of the PS.

where $E_{mF} = 2\sin(\frac{\pi}{2}\frac{d_{mF}}{w_m})$. The subscript F denotes the FZP. We obtain the normalized complex amplitude distributions if we divide both sides of Eq. (3) by $2\sin(\frac{\pi}{2}\frac{d_{mF}}{w_m})\frac{f}{f_m}$:

$$U_{mF\_\mathrm{Norm}}(R) = \exp\left[jk\left(f_m + \frac{R^2}{2f_m}\right)\right]J_0\left(\frac{kRr_m}{f_m}\right). \quad (4)$$

Suppose the FZP has M open-ring zones. In terms of the linear superposition principle, the overall diffracted light field for the FZP is given by

$$U_F(R) = \sum_{m=1}^{M} U_{mF}(R) = \sum_{m=1}^{M} E_{mF}\frac{f}{f_m}\exp\left[jk\left(f_m + \frac{R^2}{2f_m}\right)\right]J_0\left(\frac{kRr_m}{f_m}\right). \quad (5)$$

Then, we investigate the focusing property of the pinholes. Figure 3 is the schematic view of a PS and the focusing of the pinholes in the mth ring of the PS. According to [15], the analytical expression for the on-axis diffracted field of all uniformly distributed pinholes in the mth ring can be calculated by

$$U_m(R) = C_m\frac{\pi A_m f}{f_m}J_1\left(\frac{\pi}{2}\frac{d_m}{w_m}\right)\exp(jkH_0)J_0\left(\frac{kRr_m}{f_m}\right), \quad (6)$$

where C_m is a density factor for the mth pinhole ring, A_m is the constant real amplitude in the mth pinhole, d_m is the diameter of the pinholes, and $H_0 = (f^2 + R^2 + r_m^2)^{1/2}$. The parameter C_m is utilized to keep the interval of the pinholes in a ring zone. Note that Eq. (6) is valid for the condition where $N_f = \pi d_m^2/(4\lambda f) \le 0.05$, $N_m \ge 100$, and $R/r_m \le 0.05$. N_f is the Fresnel number of the pinholes, and N_m is the number of pinholes in the mth ring zone. It has been shown in [15] that the above three prerequisite conditions would be satisfied for almost all of the pinhole rings of PS, except for the several innermost pinhole rings. There are usually hundreds or thousands of small pinholes in a pinhole ring, and the focal spot for a PS is usually extremely small compared with the pinhole rings. Thus, for the overwhelming majority of pinhole rings, Eq. (6) is accurate to describe their diffracted fields. In terms of binomial expansion, H_0 could be rewritten as

$$H_0 = (f^2 + R^2 + r_m^2)^{1/2} \approx f_m + \frac{R^2}{2f_m}. \quad (7)$$

Substituting the above relation into Eq. (6), after some rearrangement, we obtain

$$U_{mP}(R) = E_{mP}\frac{f}{f_m}\exp\left[jk\left(f_m + \frac{R^2}{2f_m}\right)\right]J_0\left(\frac{kRr_m}{f_m}\right), \quad (8)$$

where $E_{mP} = C_m \pi J_1\left(\frac{\pi}{2}\frac{d_{mp}}{w_m}\right)$. The subscript P denotes the PS. The constant real amplitude A_m is taken as $A_m = 1.0$, and is omitted in Eq. (8). Next, we divide both sides of Eq. (8) by $C_m \pi J_1\left(\frac{\pi}{2}\frac{d_{mp}}{w_m}\right)\frac{f}{f_m}$, and the normalized complex amplitude distribution is

$$U_{mP\_\mathrm{Norm}}(R) = \exp\left[jk\left(f_m + \frac{R^2}{2f_m}\right)\right] J_0\left(\frac{kRr_m}{f_m}\right). \quad (9)$$

Then, the overall diffracted light field for the PS is given by

$$U_P(R) = \sum_{m=1}^{M} U_{mP}(R) = \sum_{m=1}^{M} E_{mP}\frac{f}{f_m}\exp\left[jk\left(f_m + \frac{R^2}{2f_m}\right)\right] J_0\left(\frac{kRr_m}{f_m}\right). \quad (10)$$

It is interesting to compare Eq. (4) with Eq. (9). First, it can be seen that the normalized diffraction field near the focal point of the circular open-ring zone and individual pinhole ring are identical. To the best of our knowledge, there has been no prior comparison of the normalized diffraction field. This key innovative finding overthrows the misleading former works [1], where the use of pinholes instead of open-ring zones would increase the resolution. In Fig. 4 of [1], comparisons are made between a PS and an FZP to show that the PS has better performance in terms of resolution and sidelobe suppression. In fact, the benefit of the increased resolution results from the use of a larger-diameter DOE. In works by other researchers, which increase the pinhole size by a d/w factor of 1.53, 3.51, and 5.51, a larger-aperture PS could be manufactured under the same limitation of the smallest feature that can be manufactured. According to the Rayleigh resolution formula, a higher spatial resolution could be obtained using these larger optical elements. Based on our investigation, larger-aperture FZP can also be manufactured with an increased open-ring zone width d_{mF} based on Eq. (3). Then, the larger-diameter FZP would also have better performance in terms of resolution and sidelobe suppression. A similar conclusion has been reported in [8]. However, in this paper, we investigate the essential relationship between the pinhole ring and circular open-ring zone. It should be noted that we focus only on the diffracted field near the focal region, where $R/r_m \le 0.05$ because the focal spot for a PS or FZP is usually quite small. With respect to the diffracted field of the outer regions far away from the focal point, there is indeed clear difference between the PS and FZP. However, the outer region energy that would be blocked by an optical system aperture is usually not required for the imaging.

Despite the above discussion, pure PS does have the advantage of a self-supporting structure. This property, whereby there is no disconnected material in the DOE, could benefit the imaging in x-ray microscopy, EUV lithography, and so on. Another important property of PS is the irregular distribution of pinholes, which has been utilized in [1,16,17] to reduce the higher-order contributions. However, the higher-order diffraction suppression of a quasi-random pinholes array is always accompanied by the background enhancement. Thus, we mainly focus on PSs whose holes are distributed regularly in the ring zone.

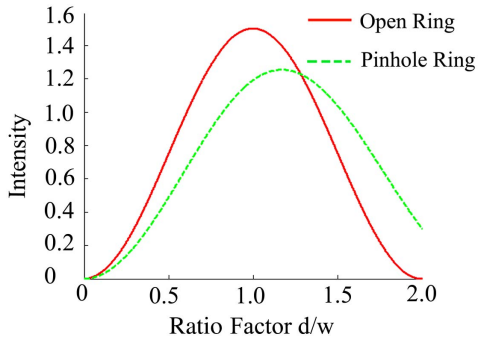

Fig. 4. Calculated focal-point intensity for open-ring zone and pinhole ring with the increase of structure sizes (normalized to the intensity of the $d_{mP}/w_m = 1.53$ pinhole ring).

Second, we investigate the diffraction efficiency. It should be emphasized that, in this study, the intensity at the focal point ($R = 0$) is utilized to compare the relative diffraction efficiency. It is the peak irradiance of the DOE. As we have proved using Eqs. (4) and (9) in Section 2, the normalized diffraction field near the focal point of an individual pinhole ring is the same as the circular open-ring zone. In such a case, the peak irradiance represents the relative efficiency of the pinhole ring and open-ring zone. Consider $C_m = 1.0$ in Eq. (8), which indicates that the pinholes in the mth ring are positioned one-by-one without any interval. By incorporating $I(R) = |U(R)|^2$, the intensity at the focal point of the individual open-ring zone and pinhole ring with the increase of the ratio factor d_{mF}/w_m and d_{mP}/w_m are calculated and plotted in Fig. 4. It can be found that, when the width of the open-ring zone is equals to the underlying width of the Fresnel zone $d_{mF}/w_m = 1.0$, the highest intensity value could be obtained. This is the case of the traditional FZP and corresponds to the maximum diffraction efficiency of an open-ring zone. From Fig. 4, instead of the commonly used $d_{mP}/w_m = 1.53$, one pinhole ring can obtain the maximum diffraction when the diameter of pinhole $d_{mP}/w_m = 1.17$. Investigation shows that the intensity value of an $d_{mF}/w_m = 1.0$ open-ring zone is 19.71% higher than that of a $d_{mP}/w_m = 1.17$ pinhole ring and 50.19% higher than that of a traditional $d_{mP}/w_m = 1.53$ pinhole ring.

Third, we focus on the apodization. From Eq. (3), it can be seen that the apodizing pupil function of the open-ring zone could be achieved with the modulation of the ratio factor d_{mF}/w_m. Compared with the open-ring zone, Eq. (8) shows that both the density factor C_m and the ratio factor d_{mP}/w_m of the pinhole ring could be utilized for the apodization. That is, PS has more flexibility for the apodization filtering. This benefit gives us more freedom during the design of the apodized DOE.

To this end, there have been full comparisons between open-ring zones of the FZP and the pinhole ring of the PS.

3. NUMERICAL SIMULATION AND ANALYSIS

In [18], it has been proven that the commercially available optical software Zemax [19] could be utilized as a good tool to evaluate the imaging performance of FZP and PS. In this section, we use the PHYSICAL OPTICS function of Zemax

to investigate the focusing property of open-ring zones and pinholes. PHYSICAL OPTICS is a powerful tool for the modeling of optical systems by propagating wavefronts. The wavefront of one beam is represented by an array of discretely sampled points, and the entire array can propagate through the optical surface. At each optical surface, a transfer function is computed, which transfers the beam from one side of the optical surface to the other. In such a case, this physical optics model enables a detailed study into the diffraction propagation of true diffractive optical systems. However, because the entire beam array must be stored during the computation, the required computational RAM would be extraordinarily large for large sampling arrays. Because of this limitation, we only use this function to investigate the performance of one 10-open-ring FZP and two 10-pinhole-ring photon sieves. Further, we use 2048 × 2048 sampling for the physical optical propagation. The focal length of the three DOEs is 100 mm and the diameter is 2.4 mm. This 10-open-ring FZP is a traditional FZP, which means that the underlying width of the open-ring zone $d_{mF}/w_m = 1.0$. With respect to the first PS, the diameter of the pinholes is $d_{mP}/w_m = 1.53$, and the density factor $C_m = 1.0$. The diameter of the pinholes in the second PS is $d_{mP}/w_m = 1.17$, and the density factor $C_m = [1.0 \times J_1(\frac{\pi}{2} \times 1.53)]/J_1(\frac{\pi}{2} \times 1.17)$. Note that the density factors for the two PSs are chosen to guarantee that the E_{mP} factors in Eq. (8) are the same. One collimated light beam with a 2.4 mm diameter and 1-W power is incident on the three DOEs. The user-defined aperture function of Zemax is utilized to define the open-ring zones and circular pinholes of the FZP and photon sieves, respectively. The footprints of the beam superimposed on the three DOEs are illustrated in Figs. 5(a)–5(c).

The 2D irradiance and Cross X irradiance at the focal point of the three DOEs are calculated using the PHYSICAL OPTIC function of Zemax. The results are shown in Figs. 6(a)–6(f). As can been seen in the figures, the profile of the irradiance near the focal point is quite the same for the three DOEs. This validates the key finding that the pinhole ring has the same normalized diffraction field near the focal region compared with the open-ring zone. Meanwhile, the peak irradiance at the focal point is 83.63 W/MM^2 for the FZP, and 55.47 W/MM^2 for the $d_{mP}/w_m = 1.53$ PS. The peak irradiance of this FZP is about 50% higher than the $d_{mP}/w_m = 1.53$ PS. This corresponds to the finding that the intensity value of an $d_{mF}/w_m = 1.0$ open-ring zone is 50.19% higher than that of a traditional $d_{mP}/w_m = 1.53$ pinhole ring. Moreover, it can be seen from Figs. 6(b), 6(c) and 6(e), 6(f) that the profiles of the irradiance and the peak irradiance are quite the same for the two PSs. This is because the E_{mP} factor is the same for the $d_{mP}/w_m = 1.53$ and $d_{mP}/w_m = 1.17$ PSs. According to our investigation, the diffracted field calculated using Eq. (8) would be the same, which proves that the diffraction field of the PS could be modulated by both the density C_m and the ratio factor d_{mp}/w_m.

To complete the discussion, the Cross X irradiance for the $\pm 0.25\lambda$ defocus of the FZP and the two PSs are also computed and are plotted in Figs. 7(a)–7(f). It can be seen that the profile of the irradiance outside the focal plane, as long as it is in the depth of focus, is also quite the same for the three DOEs. The peak irradiance at different off-focus planes of this FZP is about 50% higher than the corresponding peak irradiance of the two PSs. These comparisons validate our findings of FZP and PS in terms of spatial resolution and energy efficiency near the focal point.

It should be noted that, according to the analysis in [15], $N_f = \pi d_m^2/(4\lambda f) \le 0.05$, $R/r_m \le 0.05$, and $N_m \ge 100$ are the three prerequisites for the validity of the pinhole ring model. Technically, the pinholes for several innermost pinhole rings of the two PSs do not meet all of these requirements simultaneously. In the strictest sense, there is little difference between the normalized irradiance of the FZP and that of the two PSs. However, as can be seen from Figs. 6 and 7, the difference in the overall diffracted field is relatively small and can be explained as follows. Equations (3) and (8) are obtained based on some approximations during the numerical deduction. The validity ranges are given to guarantee the calculation accuracy. For several innermost pinhole rings, the diffracted fields that are calculated using Eqs. (3) and (8) are slightly different compared with the actual diffracted field. In spite of the subtle difference, the overall profile of the irradiance of the FZP and that of the two PSs appears similar. In fact, with the decreased pinhole diameter and the increase in the number of pinholes, the normalized diffracted field at the focal point of the individual pinhole ring would become close to that of one open-ring zone. These comparisons are further validated in Section 4.

In this section, by performing modeling using Zemax, we proved that the normalized diffraction field near the focal point of the individual pinhole ring and the circular open-ring zone appears to be the same. Besides, open-ring zones have superior performance in terms of energy efficiency. Last but not least, the profile of the irradiance near the focal point of the PS could be modulated by the pinhole density C_m and d_{mP}/w_m. In contrast, the apodizing pupil function of the FZP open-ring zone

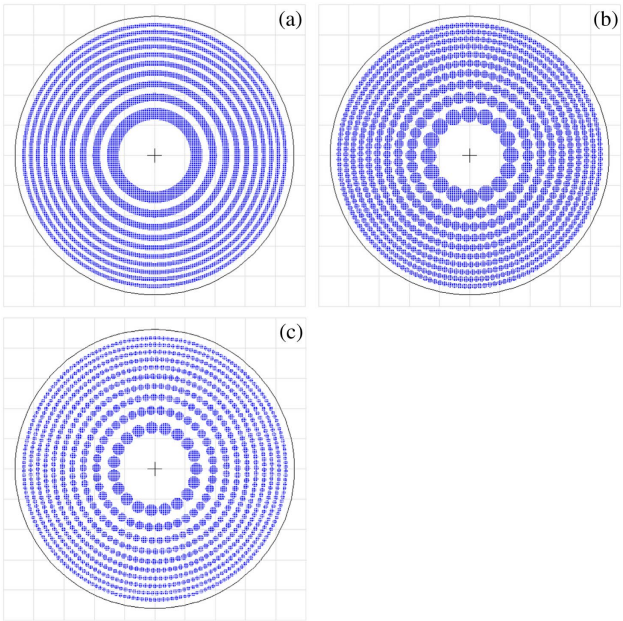

Fig. 5. Footprint of the 2.4 mm diameter beam, which is superimposed on the (a) FZP, (b) $d_{mP}/w_m = 1.53$ PS, and (c) $d_{mP}/w_m = 1.17$ PS.

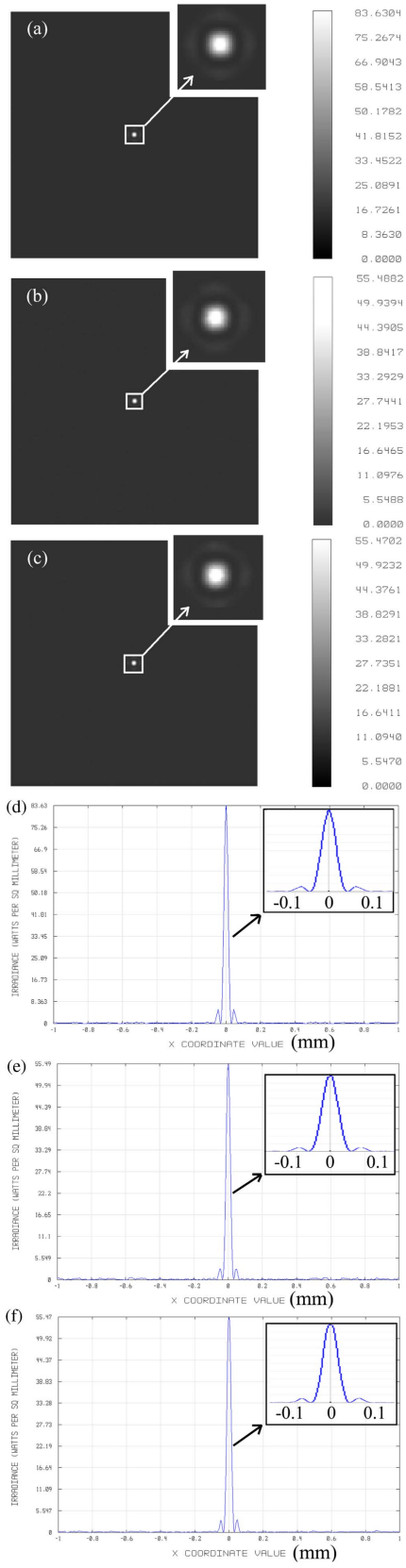

Fig. 6. 2D irradiance at the focal plane for (a) FZP, (b) the $d_{mP}/w_m = 1.53$ PS, and (c) the $d_{mP}/w_m = 1.17$ PS. Cross X irradiance for (d) FZP, (e) the $d_{mP}/w_m = 1.53$ PS, and (f) the $d_{mP}/w_m = 1.17$ PS.

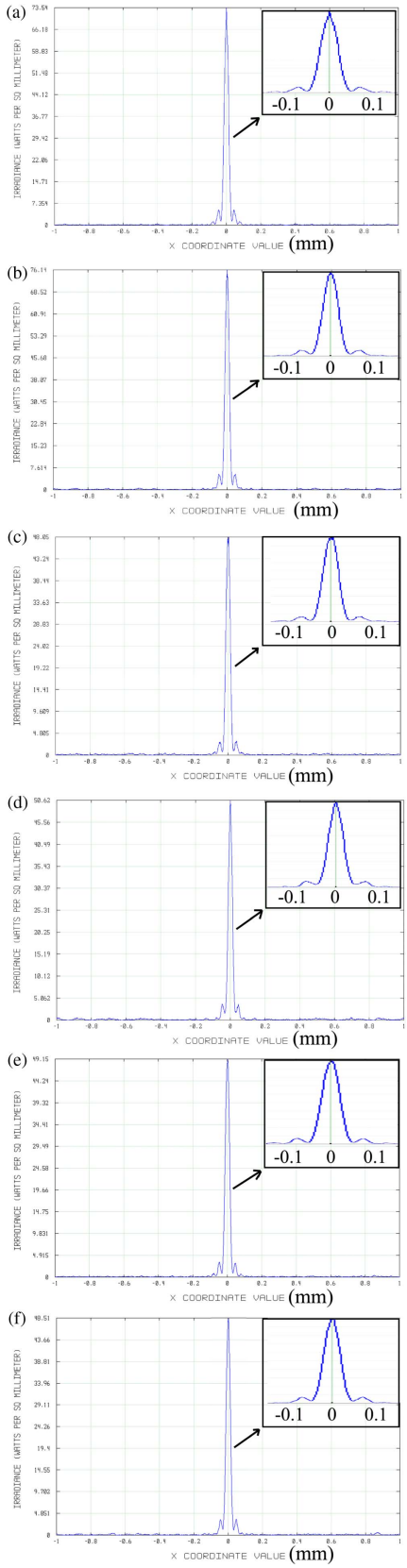

Fig. 7. (a) and (b) are the Cross X irradiance at the $\pm 0.25\lambda$ off-focus plane for the FZP; (c) and (d) are the Cross X irradiance at the $\pm 0.25\lambda$ off-focus plane for the $d_{mP}/w_m = 1.53$ PS; and (e) and (f) are the Cross X irradiance at the $\pm 0.25\lambda$ off-focus plane for the $d_{mP}/w_m = 1.17$ PS.

could only be achieved with the modulation of the ratio factor d_{mF}/w_m. This means that the use of the PS has a greater advantage during the apodization filter design. In order to combine the benefits of open-ring zones and pinhole rings, an apodized diffractive optical element composed of open-ring zones and pinholes has been proposed. Investigations in Section 4 show that the energy efficiency is increased, and the manufacturing difficulty could be reduced.

4. DESIGN OF APODIZED DIFFRACTIVE OPTICAL ELEMENT COMPOSED OF OPEN-RING ZONES AND PINHOLES

In the above discussion, the nature of the relationship between open-ring zones of FZP and the pinhole rings of a PS was investigated. Based on the benefits and deficiencies of these two DOEs, we propose the design example of an apodized diffractive optical element composed of open-ring zones and pinholes. It is a two-region compound APS (CAPS) that combines open-ring zones in the inner region and pinholes in the outer region. The design process of the CAPS may be described as follows. First, people could choose their own specific apodization window for sidelobe suppression or other purposes. Once the apodization window is chosen, apodized open-ring zones are utilized in the inner region. The initial unapodized ratio factor is set to $d_{mF}/w_m = 1.0$ in order to obtain the maximum diffraction efficiency to the focal point. Combing the apodization window $G(r_m)$, the width of each apodized open-ring zone d_{mF} can be calculated by solving

$$G(r_m) = \left[2 \sin\left(\frac{\pi}{2}\frac{d_{mF}}{w_m}\right)\right] \Big/ \left[2 \sin\left(\frac{\pi}{2}\right)\right]. \tag{11}$$

In the outer region, apodized pinhole rings are used instead. With respect to these outer pinholes, the ratio factor $d_{mP}/w_m = 2.0$ is chosen. This means that the diameter of the pinhole is twice that of the underlying Fresnel zone. This could maximize the pinhole sizes and significantly relax the fabrication requirements. Then, the density factor C_m can be calculated by solving

$$G(r_m) = \left[C_m \pi J_1\left(\frac{\pi}{2} \times 2\right)\right] \Big/ \left[2 \sin\left(\frac{\pi}{2}\right)\right]. \tag{12}$$

It should be noted that the values of C_m should be smaller than 1.0 so as to guarantee no overlapping of pinholes in individual ring zones. This $C_m \le 1.0$ could be utilized as the criterion for choosing the boundary between the two regions. Then, the pinhole numbers for each ring zone can be given by

$$N = C_m \frac{2\pi}{d_m/r_m}. \tag{13}$$

To validate the proposed methodology, we designed another classic APS. Both the CAPS and APS have the same aperture $D = 40$ mm, focal length $f = 100$ mm, and working wavelength 632.8 nm. The Gaussian apodization window

$$G(r_m) = \exp[-2r_m^2/(D/2)^2] \tag{14}$$

is chosen. The pinhole diameter for the classic APS is $d_{mP} = 1.53w_m$. By performing calculations, each of the two DOEs has 3129 rings. The diameter of the pinholes in classic $d_{mP}/w_m = 1.53$ APS monotonously decreases for the 3129 pinhole rings. With respect to the CAPS, according to the apodization matching condition, it can be written

$$\exp[-2r_m^2/(D/2)^2] = \left[C_m \pi J_1\left(\frac{\pi}{2} \times 2\right)\right] \Big/ \left[2 \sin\left(\frac{\pi}{2}\right)\right]. \tag{15}$$

Note that the values of C_m should be smaller than 1.0 to prevent the overlapping of pinholes in individual ring zones. By substituting $C_m = 1.0$ into Eq. (15), it can be calculated that the boundary is $r_m = 12.69$ mm, which corresponds to $m = 1628$. Thus, in the inner region of CAPS, there are open-ring zones for $m = 1 - 1627$. For the outer region $m = 1628 - 3129$, pinhole rings are utilized instead.

It is impossible to draw the overall 3129 rings of diffraction structures in a single picture because the structures in the outer rings would be too small to be distinguished. In order to give an intuitive impression, the layouts of one 27-ring CAPS and one classic 27-ring APS are schematically shown in Fig. 8 for comparison. Figures 8(a) and 8(b) are only used to graphically illustrate the layout of CAPS and APS and are not part of the 3129 ring diffractive elements. In Fig. 8(a), the sizes of the pinholes in classic APS monotonously decrease with an increased number of rings. The pinhole diameter for the classic APS is $d_{mP} = 1.53w_m$. In comparison, there is an obvious change from the open-ring zone to pinholes for the two angular regions of CAPS in Fig. 8(b). It can be seen that the structure sizes of pinholes in the outer rings of CAPS are larger than that in classic APS. The increase of the pinhole size is owing to the ratio factor $d_{mP}/w_m = 2.0$ for the outer rings of CAPS. This reduces the cost and difficulties involved in fabricating microstructure pinholes. On the other hand, a larger-aperture PS could be manufactured under the same limitation of the smallest feature that can be manufactured.

The diffracted field near the focal point on the focal plane of CAPS and the classic APS are calculated using Eqs. (5) and (10).

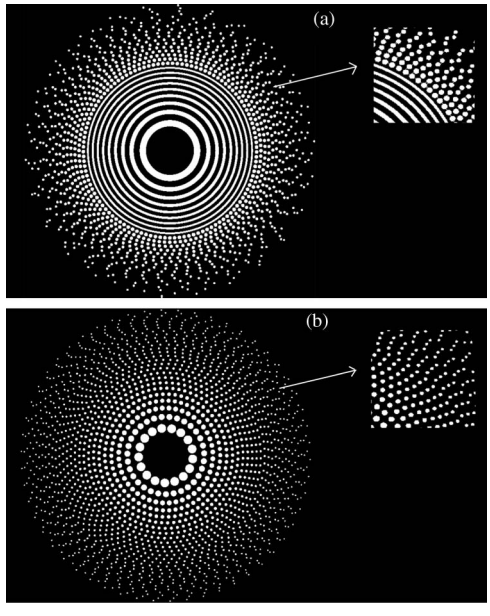

Fig. 8. Schematic illustration of (a) CAPS and (b) classic APS.

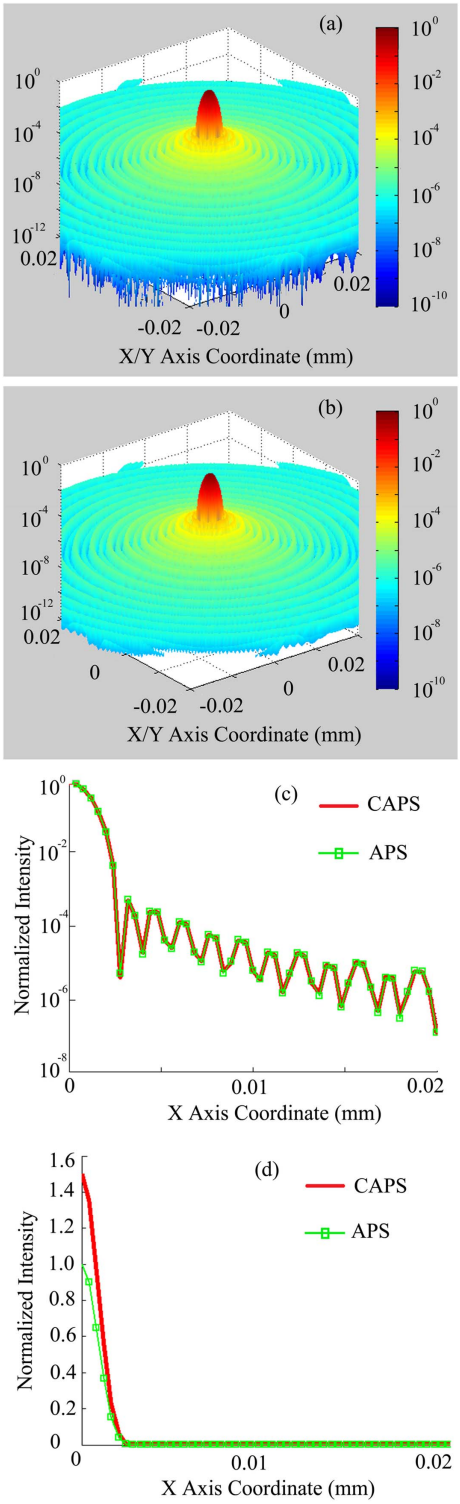

Fig. 9. (a) and (b) 3D surface plots of the intensity distribution of CAPS and the classic APS, respectively. (c) and (d) Cross X intensity distribution of CAPS and classic APS. In (a)–(c), the intensities are normalized to the individual peak intensity and the plot is on the logarithmic scale. In (d), the intensities of CAPS and classic APS are normalized to the peak intensity of the classic APS. The plot in (d) is linear.

The intensity distributions are illustrated in Figs. 9(a)–9(d). In Figs. 9(a) and 9(b), the 3D surface plots of the intensity distribution near the focal point of CAPS and the classic APS are, respectively, shown. Figure 9(c) is a comparison of the Cross X intensity distribution between CAPS and classic APS. The intensities in Figs. 9(a)–9(c) are normalized to the individual peak intensity, and the plot is on the logarithmic scale. From Figs. 9(a)–9(c), it can be seen that the normalized intensity distributions near the focal point of the two PSs are in good agreement, which means that the two diffractive elements have the same resolution. As previously discussed, this is because the two elements have the same diameter. The intensities in Fig. 9(d) are normalized to the peak intensity of the classic $d_{mP} = 1.53w_m$ APS. Analysis shows that the peak intensity of the CAPS is increased by 50.19%, and these modeling results validate the high performance of CAPS in terms of energy efficiency. Meanwhile, the high spatial resolution and sidelobe suppression have been maintained for CAPS. Besides, the width of the CAPS innermost open-ring zone, where $r_1 \approx 0$ and $G(r_1) \approx 1.0$, equals the underlying width of the first Fresnel ring zone. According to Eq. (3), this open-ring zone has the highest constructive contribution to the focus. In addition, the parameters in the outer regions are determined by the apodization matching condition. In conclusion, once the element diameter and the apodization window are chosen, this innovative compound PS CAPS has the maximum diffraction efficiency. It is worth reminding that the maximum diffraction efficiency defined here is utilized to describe the diffraction property of the apodized DOE with specific apodized pupil function and element diameter. According to our investigation in Section 2, the unapodized traditional FZP with $d_{mF}/w_m = 1.0$ would have an even higher diffraction efficiency. However, traditional FZPs are unapodized and have problems, including manufacturing complexity and sidelobes.

The widths of the open-ring zones d_{mF} and the diameter of pinholes d_{mP} are shown in Fig. 10. The figure clearly illustrates that the sizes of the pinholes in classic APS monotonously decrease with an increase in the number of rings. The smallest diameter is in the outmost ring, and the size is 2.47 μm. With respect to the optimized CAPS, there is a jump at the boundary between the two regions. This jump is related to the change from the open-ring zones to the $d_{mP}/w_m = 2.0$ pinhole rings during the design of the CAPS. Clearly, the pinholes in ring order $m = 1268 - 3129$ of CAPS have larger diameters than that in classic APS. Further, the widths of

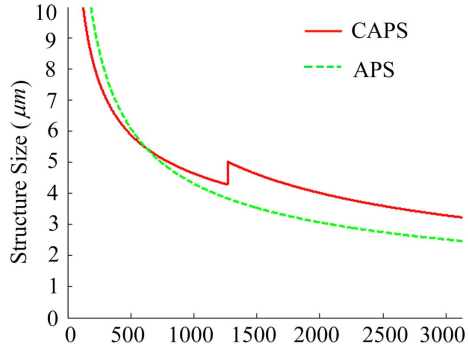

Fig. 10. Structure sizes of the CAPS and the classic APS.

the 626–1267 open-ring zones are also larger than the diameter of the corresponding pinhole rings owing to the modulation of the ratio factor d_{mF}/w_m. The increase of the structure size could be beneficial to the manufacturing process. Analysis shows that the smallest pinhole size for the optimized CAPS is 3.23 μm, which is 30.77% larger than the smallest size in classic APS.

In the above analysis, we focus our discussion only on the first-order diffraction, which means that the size $d_{mP} \le 2w_m$ and $d_{mF} \le 2w_m$. Obviously, a higher-order diffraction, which further increases the size of the microscale structures, could be utilized for diffractive focusing. However, one main defect is that the diffraction efficiency would be significantly reduced owing to the high-order diffraction. Besides, this nonimaging high-order diffraction would create stray light that decreases the imaging contrast. Nevertheless, the focusing property of higher-order FZP open-ring zones and PS pinhole rings could still be described by Eqs. (5) and (10).

5. CONCLUSION

In this paper, we investigated the nature of the relationships between open-ring zones of FZP and the pinhole rings of PSs. First, we proved that the normalized diffraction fields near the focal point of the open-ring zone and pinhole ring are the same. Second, it has been shown that the open-ring zones of FZP have higher energy efficiency. Third, when utilized in apodization filtering, the modulation of the pinhole rings shows superior performance compared with open-ring zones.

Based on our investigation, a novel high-performance apodized diffractive optical element composed of open-ring zones and pinholes has been proposed. The CAPS combines the benefits of FZP and PS. We showed that, when the apodized pupil function and element diameter are determined, the maximum optimal energy concentration at the focusing field can be achieved for CAPS. Compared with the traditional $d/w = 1.53$ apodized PS, the CAPS has a 50.19% higher energy efficiency, and the minimum pinhole size is enlarged by 30.77%. Meanwhile, the two apodized DOEs have the same form of normalized intensity distribution near the focal point at the focal plane.

It should be noted that the focal spot for PS and FZP are usually quite small. The diffracted field of the outer regions far away from the focal point would usually be blocked by the optical system aperture and would not enter the imaging path. Thus, in this paper, we only discussed the diffracted field near the focal region. Besides, it should be noted that the CAPS requires a substrate, which is not the case for a pure PS element. Nevertheless, the methodology employed in this study could be utilized as a basis for the design of the apodized DOEs. This paper may benefit research into apodized DOEs in terms of realizing increased resolution, sidelobe depression, and reduced manufacturing complexity.

Funding. National Natural Science Foundation of China (NSFC) (61505201, 61605016, 51775531); Science and Technology Development Plan of Jilin Province, China (20160520175JH).

REFERENCES AND NOTES

1. L. Kipp, M. Skibowski, R. L. Johnson, R. Berndt, R. Adelung, S. Harm, and R. Seemann, "Sharper images by focusing soft x-rays with photon sieve," Nature **414**, 184–188 (2001).
2. W. Chao, B. D. Harteneck, J. A. Liddle, E. H. Anderson, and D. T. Attwood, "Soft x-ray microscopy at a spatial resolution better than 15 nm," Nature **435**, 1210–1213 (2005).
3. C. Xie, X. Zhu, L. Shi, and M. Liu, "Spiral photon sieves apodized by digital prolate spheroidal window for the generation of hard-x-ray vortex," Opt. Lett. **35**, 1765–1767 (2010).
4. G. Cheng, C. Hu, P. Xu, and T. Xing, "Zernike apodized photon sieves for high-resolution phase-contrast x-ray microscopy," Opt. Lett. **35**, 3610–3612 (2010).
5. R. Menon, D. Gil, G. Barbastathis, and H. I. Smith, "Photon-sieve lithography," J. Opt. Soc. Am. A **22**, 342–345 (2005).
6. C. Xie, X. Zhu, and J. Jia, "Focusing properties of hard x-ray photon sieves: three-parameter apodization window and waveguide effect," Opt. Lett. **34**, 3038–3040 (2009).
7. G. Andersen, "Large optical photon sieve," Opt. Lett. **30**, 2976–2978 (2005).
8. Q. Cao and J. Jahns, "Focusing analysis of the pinhole photon sieve: individual far-field model," J. Opt. Soc. Am. A **19**, 2387–2393 (2002).
9. G. Anderson and D. Tullson, "Broadband antihole photon sieve telescope," Appl. Opt. **46**, 3706–3708 (2007).
10. Z. Chen, C. Wang, D. Pu, J. Hu, and L. Chen, "Ultra-large multi-region photon sieves," Opt. Express **18**, 16279–16288 (2010).
11. M. J. Simpson and A. G. Michette, "Imaging property of modified Fresnel zone plates," Opt. Acta **31**, 403–413 (1984).
12. O. Hofsten, M. Bertilson, J. Reinspach, A. Holmberg, H. M. Hertz, and U. Vogt, "Sub-25-nm laboratory x-ray microscopy using a compound Fresnel zone plate," Opt. Lett. **34**, 2631–2633 (2009).
13. C. Xie, X. Zhu, H. Li, L. Shi, and Y. Wang, "Feasibility study of hard-x-ray nanofocusing above 20 keV using compound photon sieves," Opt. Lett. **35**, 4048–4050 (2010).
14. Q. Cao and J. Jahns, "Modified Fresnel zone plates that produce sharp Gaussian focal spots," J. Opt. Soc. Am. A **20**, 1576–1581 (2003).
15. T. Liu, X. Zhang, L. Wang, Y. Wu, J. Zhang, and H. Qu, "Multi-region apodized photon sieve with enhanced efficiency and enlarged pinhole sizes," Appl. Opt. **54**, 7175–7180 (2015).
16. F. Giménez, J. A. Monsoriu, W. D. Furlan, and A. Pons, "Fractal photon sieve," Opt. Express **14**, 11958–11963 (2006).
17. A. Sabatyan and P. Roshaninejad, "Super-resolving random- 410 Gaussian apodized photon sieve," Appl. Opt. **51**, 6315–6318 (2012).
18. Z. Chen, C. Wang, and H. Qu, "Imaging characterization and tolerance analysis of thin planar photon sieves," Proc. SPIE **7284**, 72840J (2009).
19. ZEMAX optical system design software was developed and distributed by ZEMAX Development Corporation, 3001 112th Avenue NE, Suite 202, Bellevue, Washington 98004-8017, USA.